ChemPubSoc Europe

FULL PAPERS

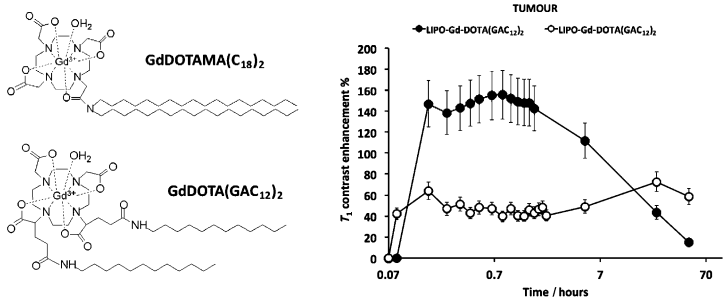

Creating an image: The in vivo performance of liposomes loaded with different amphiphilic Gd-based magnetic resonance imaging agents is compared in a tumour model on mice. The tetracarboxylic complex GdDOTA(GAC_{12})$_2$ (see figure), which combines a fast rate of water exchange and a restricted local mobility, shows the highest sensitivity detection and more favourable pharmacokinetic properties.

*E. Cittadino, M. Botta, L. Tei, F. Kielar, R. Stefania, E. Chiavazza, S. Aime, E. Terreno**

■■ – ■■

In Vivo Magnetic Resonance Imaging Detection of Paramagnetic Liposomes Loaded with Amphiphilic Gadolinium(III) Complexes: Impact of Molecular Structure on Relaxivity and Excretion Efficiency

DOI: 10.1002/cplu.201300096

In Vivo Magnetic Resonance Imaging Detection of Paramagnetic Liposomes Loaded with Amphiphilic Gadolinium(III) Complexes: Impact of Molecular Structure on Relaxivity and Excretion Efficiency

Evelina Cittadino,[a] Mauro Botta,[b] Lorenzo Tei,[b] Filip Kielar,[b] Rachele Stefania,[a] Enrico Chiavazza,[a] Silvio Aime,[a, c] and Enzo Terreno*[a, c]

The magnetic resonance imaging (MRI) performance of two liposome formulations incorporating amphiphilic 1,4,7,10-tetraazacyclododecane-1,4,7,10-tetraacetic acid (DOTA)-like Gd^{III} complexes has been investigated both in vitro and in vivo. The complexes differ in one donor group of the coordination cage (carboxylate versus carboxoamide), and in the length (C_{12} versus C_{18}) and the point of attachment of the aliphatic chains to the chelators. The in vitro ^1H relaxometric characterisation of the systems, performed with a newly developed relaxation model that takes into account the contributions of the Gd^{III} chelates pointing in- and outwards of the liposome, indicates that their efficacy is optimal in the range 0.5–1.5 T. The tetracarboxylic C_{12}-containing liposomes (LIPO-GdDOTA(GAC_{12})$_2$; GA = glutaric acid) are four-fold more efficient than the monoamide C_{18}-based analogue (LIPO-GdDOTAMA(C_{18})$_2$). Such a difference is also found in vivo at 1 T in a melanoma tumour model on mice. A few hours after intravenous injection, the T_1 contrast enhancement in the organs where the nanovesicles typically distribute (liver, spleen, kidneys and tumour) is much higher for LIPO-GdDOTA(GAC_{12})$_2$. Interestingly, after about 7 h post-injection the contrast enhancement observed for the more efficient liposomes decreases rapidly and becomes lower than for LIPO-GdDOTAMA(C_{18})$_2$. The relaxometric data and the quantification of the Gd^{III} complexes in the organs, determined ex vivo by inductively coupled plasma mass spectrometry, indicate that: 1) the differences in the contrast enhancement can be attributed to the different rate of water exchange and rotational dynamics of the Gd complexes, and 2) the rapid contrast decrease is caused by a faster clearance of GdDOTA(GAC_{12})$_2$ from the organs. This is also confirmed by using a newly synthesised amphiphilic cyanine-based fluorescent probe (Cy5-(C_{16})$_2$). As one of the main limitations for the clinical translation of liposomes incorporating amphiphilic imaging agents is related to their very long persistence in the body, the results reported herein suggest that the clearance of the probes can be accelerated, without compromising their role, by a proper selection of the lipophilic portion of the incorporated compound as well as of the ligand site at which the aliphatic tails are linked. Then, GdDOTA(GAC_{12})$_2$ complex may represent a good candidate for the development of improved MRI protocols based on paramagnetically labelled lipidic nanoparticles.

Introduction

Magnetic resonance imaging (MRI) is one of the most powerful non-invasive medical diagnostic procedures currently in use. The superb spatial resolution and the outstanding capacity of differentiating soft tissues justify the steadily growing clinical relevance of this imaging modality. MRI is based on the detection of the NMR signal generated by water protons. Through specific pulse sequences, the contrast is generated wherever there is a difference in the longitudinal (T_1) or transverse (T_2) relaxation times of tissue ^1H_2O. As the relaxation times are extremely sensitive to the biological environment of water molecules, the MRI contrast can report on many structural and dynamic alterations associated with pathological states, even without using exogenous contrast media.[1] However, if the endogenous contrast between healthy and pathological regions is poor, or if the imaging experiment is aimed at visualising molecular events, the administration of imaging reporters becomes mandatory.[2] Clinically approved MRI contrast agents are classified as T_1 or T_2 agents; the former group includes paramagnetic Gd^{III}- or Mn^{II}-based complexes,[3] whereas the second class mainly comprises superparamagnetic iron oxide (SPIO) particles.[4]

The challenge of designing new highly sensitive T_1 agents has been pursued mainly through two approaches: 1) optimisation of the dynamic and structural determinants that define the efficacy to generate contrast by a single paramagnetic

[a] Dr. E. Cittadino, Dr. R. Stefania, E. Chiavazza, Prof. S. Aime, Prof. E. Terreno
Department of Molecular Biotechnology and Health Sciences
Molecular Imaging Center, Università di Torino
Via Nizza 52, 10126 Torino (Italy)
E-mail: enzo.terreno@unito.it

[b] Prof. M. Botta, Dr. L. Tei, Dr. F. Kielar
Department of Scienze e Innovazione Tecnologica
Università del Piemonte Orientale "Amedeo Avogadro"
Viale T. Michel 11, 15121 Alessandria (Italy)

[c] Prof. S. Aime, Prof. E. Terreno
Center for Preclinical Imaging, University of Torino
Via Ribes 5, 10010 Colleretto Giacosa, Torino (Italy)

centre, and 2) increasing the number of paramagnetic units that can be delivered to a given biological target. The ability of the paramagnetic agent to create T_1 contrast in vivo is typically predicted by the value of its in vitro relaxivity (r_1), which corresponds to the paramagnetic longitudinal relaxation rate of solvent water protons normalised to one millimolar concentration of agent.[3] The r_1 value has to be referred to a given magnetic field strength, temperature and pH. In the last two decades, great efforts have been made to shed light on the molecular mechanisms underlying the paramagnetic relaxation, thus making possible the rational design of MRI probes with improved sensitivity.[3,5] However, MRI visualisation of low-concentration targets invariably implies the need to deliver a high number of agent molecules. In turn, this requires that a number of paramagnetic complexes have to be loaded on a suitable carrier. In this regard, nanotechnology offers a wide portfolio of nanocarriers including dendrimers, micelles, liposomes, solid lipid nanoparticles, nanoemulsions and other forms of lipophilic aggregates as well as natural systems, such as apoferritin, lipoproteins, viral capsids and even cells.[5,6] Important properties to be considered for the selection of the most appropriate nanocarrier are size, biocompatibility and biological stability.[7]

Among the above-cited nanosystems, liposomes combine several particular favourable properties. They are nanovesicles (typical size between 50 and 200 nm) formed by a unilamellar phospholipid-based bilayer entrapping an aqueous core. The main advantages of liposomes are: 1) high biocompatibility; 2) easiness of preparation; 3) great chemical versatility (ability to be loaded with hydrophobic, amphiphilic and hydrophilic substances); 4) simplicity of decorating the surface (with targeting vectors, blood lifetime modulators, drugs, diagnostic tracers and so forth); and 5) a longstanding and well-established clinical use as drug-delivery carriers.[8] In analogy to all the other nanocarriers, liposomes can also distribute passively in pathological areas characterised by an altered endothelial permeability, such as solid tumours, atherosclerotic plaques and inflammation sites, through the so-called enhanced permeability and retention (EPR) mechanism.[9] For all these reasons, liposomes are excellent candidates for developing highly sensitive MRI agents, especially in the emerging field of theranosis.[10] There are two main approaches to design liposomal MRI agents depending on whether the imaging reporter is encapsulated in the aqueous core or incorporated in the bilayer. The latter option appears preferable if one seeks high-sensitivity systems. In fact, it is well established that the relaxivity of a paramagnetic centre, especially at magnetic field strengths higher than 0.1 T, is mainly controlled by the rotational tumbling (τ_R) of the complex, which is correlated to the size of the nanocarrier and the overall rigidity of the agent–nanosystem linkage.[5] To facilitate the incorporation of the paramagnetic chelate into the liposome bilayer, an appropriate balance between the hydrophilic and the hydrophobic portions of the agent is necessary. So far, two types of amphiphilic paramagnetic complexes have been investigated and used to a great extent. These are based on: 1) an acyclic diethylenetriaminepentaacetic acid (DTPA)-like cage in which the linkage of two aliphatic chains involves the transformation of two terminal coordinating carboxylates into amide functionalities (e.g., DTPA–bovine serum albumin);[8,11,12] or 2) a macrocyclic 1,4,7,10-tetraazacyclododecane-1,4,7,10-tetraacetic acid (DOTA)-like cage in which the hydrocarbon tails are conjugated through an amide linkage to a single coordinating carboxylate.[8,12,13] DTPA amides have been used extensively because of the relative ease of syntheses, but their Gd^{III} complexes are characterised by a relatively low thermodynamic and kinetic stability, which prevents their clinical translation. In addition, the transformation of two carboxylic groups into carboxoamides inevitably causes a remarkable elongation of the exchange lifetime (τ_M) of the water molecule coordinated to the paramagnetic ion, which negatively affects the relaxivity enhancement expected upon slowing down the rotational motion of the agent.[11] Conversely, monofunctionalised DOTA-like structures possess markedly higher thermodynamic and kinetic stabilities and exhibit good ability to generate contrast. The relaxivity of such agents can be further improved through a rational design of the conjugation linkage between the complex and the aliphatic tails. Another important property that influences the clinical potential of these agents is represented by the body clearance rate. Typically, the amphiphilic agents developed so far contain C_{16} or C_{18} hydrocarbon tails that stabilise the liposomal incorporation, but confer an undesirable very slow clearance from the tissues where the liposomes accumulate, especially in liver and spleen. Recently, a new amphiphilic GdDOTA-like agent bearing shorter hydrophobic chains (C_{12}), suitably designed to display optimal τ_M and τ_R values, was proposed (Scheme 1).[14] The presence of two aliphatic chains on adjacent coordinating arms was conceived to reduce considerably the local rotational motion of the Gd^{III} chelates incorporated in the liposome bilayer.

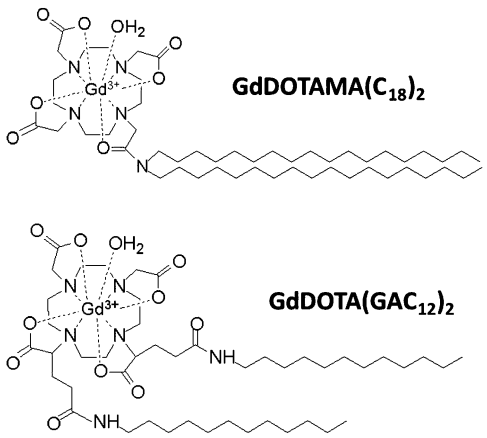

Scheme 1. The amphiphilic Gd^{III} complexes investigated in this work.

In this work, we investigated the in vitro (relaxometry) and in vivo (melanoma tumour model on mice) MRI performance of liposomes incorporating either this complex (LIPO-GdDOTA-$(GAC_{12})_2$) (LIPO = liposome, GA = glutaric acid) or an amphiphilic monoamide Gd^{III} agent conjugated with C_{18} chains (LIPO-GdDOTAMA$(C_{18})_2$) as a reference.[13] The two complexes are shown in Scheme 1.

Results and Discussion

In vitro relaxometric characterisation of the liposomal agents

The magnetic field dependence of the longitudinal ^{1}H relaxivity of the two paramagnetic liposomes was measured at 298 K over the range 2.343×10^{-4}–1.645 T, which corresponds to proton Larmor frequencies varying between 0.01 and 70 MHz. The experimental data are shown in Figure 1 and constitute the so-called nuclear magnetic relaxation dispersion (NMRD)

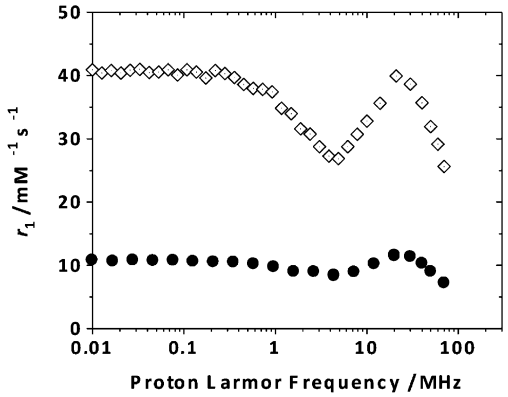

Figure 1. ^{1}H NMRD profiles of LIPO-GdDOTAMA(C_{18})$_2$ (●) and LIPO-GdDOTA-(GAC_{12})$_2$ (◇) at 298 K.

profiles, characterised by well-defined amplitude and shape representing a sort of fingerprint that describes the relaxometric behaviour of the sample. The NMRD profiles of LIPO-GdDOTA(GAC_{12})$_2$ and LIPO-GdDOTAMA(C_{18})$_2$ clearly show a marked relaxivity difference over the entire frequency range investigated, and their shape is rather similar and typical of macromolecular systems characterised by a reduced rotational tumbling rate.[3,5]

We can distinguish: 1) a region of constant relaxivity at low fields (≈0.01–0.5 MHz); 2) a dispersion around 1–3 MHz; 3) a peak centred about 20–30 MHz; and 4) a steep decrease of r_1 at higher fields. However, although for LIPO-GdDOTAMA(C_{18})$_2$ the r_1 peak ($r_1=11.4$ mM^{-1}s^{-1}) is broad and centred at 30 MHz, for LIPO-GdDOTA(GAC_{12})$_2$ it is narrower and with a maximum at 20 MHz ($r_1=40.0$ mM^{-1}s^{-1}). The Δr_1 between the two paramagnetic liposomes is large and shows a tendency to decrease slightly with increasing frequency: it assumes the value of approximately 30 mM^{-1}s^{-1} at 0.01 MHz, 28 mM^{-1}s^{-1} at 20 MHz and 21 mM^{-1}s^{-1} at 60 MHz. These results highlight clearly the superior relaxometric performance of the liposomes loaded with GdDOTA(GAC_{12})$_2$ relative to the liposome formulation based on the GdDOTAMA(C_{18})$_2$ complex. This difference reproduces well that observed in micellar systems formed by these two lipophilic complexes, that is, $r_1=30.9$ mM^{-1}s^{-1} for GdDOTA(GAC_{12})$_2$[14] and approximately 20 mM^{-1}s^{-1} for GdDOTAMA(C_{18})$_2$,[13] at 20 MHz and 310 K. In qualitative terms, we can explain the difference in relaxivity on the basis of the different rates of bound water exchange ($k_{ex}=1/\tau_M$) of the complexes and of the different degree of local rotational flexibility (τ_{RL}). The residence lifetime τ_M is known to be significantly different for this type of DOTA-like complex: at 298 K the anionic complex typically exhibits values of the order of 100–300 ns, whereas the neutral complex is characterised by values that are longer by a factor of 3–4. It is well recognised that a long τ_M value ($\geq$0.5 μs) may severely limit the relaxivity, especially when the complex has a restricted rotational motion.[5,15] The occurrence of a local rotational motion about the linker connecting the coordination cage of the Gd chelate and the anchoring site on the nanoparticle represents a second relevant factor that limits the r_1 of macromolecular systems. The local motion is usually much faster than the global rotation of the nanoparticle ($\tau_{RL}<\tau_{RG}$), thus giving rise to a shorter effective τ_R that lowers r_1. From this perspective, a reduced rotational flexibility is expected for GdDOTA(GAC_{12})$_2$ in which the two aliphatic chains are positioned on two adjacent acetic arms, therefore achieving the so-called multisite attachment.[14,16]

For a more accurate and quantitative interpretation aimed at identifying in detail the reasons for the different relaxivity of the two systems, we need to analyse the observed NMRD profiles in terms of the paramagnetic relaxation theory. Typically, the data are fitted by using the equations for the inner (IS) and outer hydration sphere (OS) contributions to relaxivity.[3b] The former arises from the time-dependent dipolar interaction between the electron (Gd^{III}) and nuclear (protons of the coordinated water molecule) magnetic moments and is based on the classical Solomon–Bloembergen–Morgan (SBM) theory.[3] The time modulation involves rotation of the complex (τ_R), electron magnetic moment relaxation ($T_{1,2e}$) and chemical exchange of the bound water molecule with bulk water (k_{ex}). The second contribution, determined by solvent molecules diffusing near the paramagnetic complex, depends on the relative diffusion coefficient D of solute and solvent molecules and their distance of closest approach a, and it is described by Freed's equation.[17] The OS contribution is much smaller than the IS relaxivity and in a first approximation could be neglected. However, the direct application of the SBM and Freed theories is not entirely justified in the case of liposomes in which there are contributions to r_1 derived either from the complexes that point towards the interior of the vesicles or by complexes with the coordination cage pointing outwards, that is [Eq. (1)]:

$$r_1 = {R_{1p}}^{IN} + {R_{1p}}^{OUT} \quad (1)$$

For this reason, we have developed a model that explicitly takes into account these two conditions.

The basic concept is that the Gd^{III} complexes exposed on the external leaflet of the bilayer directly affect the nuclear magnetic relaxation rate of the bulk water protons, which are by far the predominant fraction of water in the liposomal suspension (>98% under the experimental conditions used in this work). Hence, for monoaqua complexes such as those considered herein [Eq. (2)]:

$$R_{1p}^{OUT} = \left(\frac{\chi_{Gd}^{OUT} \times 10^{-3}}{55.6} \times \frac{1}{T_{1M} + \tau_M}\right) + R_{1OS}^{OUT} \quad (2)$$

in which $\chi_{Gd}{}^{OUT}$ is the molar fraction of the Gd complex pointing outward of the liposomes, T_{1M} is the relaxation time of the protons of the Gd-bound water molecule, τ_M is their mean residence lifetime, and $R_{1OS}{}^{OUT}$ is the outer-sphere relaxivity contribution. Both IS and OS contributions were modelled according to the classical SBM and Freed theories, suitably modified using the model-free Lipari–Szabo description of the rotational dynamics.[19] This allows the separation of the local molecular rotation of the chelates (characterised by the correlation time τ_{RL}) from the global tumbling motion of the nanoparticle (τ_{RG}). The degree of correlation between the two types of motion is described by the order parameter S^2 ($0 < S^2 < 1$).

On the other hand, the relaxivity contribution to the bulk water compartment from the Gd complexes pointing inward of the liposomes, $R_{1p}{}^{IN}$, can be described on the basis of the model first proposed by Fossheim et al.,[19] suitably adapted to the case of a paramagnetic agent incorporated into the bilayer.

According to this model, bulk water protons receive a relaxation contribution from the water protons in the inner core of the vesicles that is proportional to the volume fraction of the intra-liposomal pool ($\chi^{INTRALIPO}$), and dependent on both the relaxation time of the protons entrapped in the liposomes ($T_1{}^{INTRALIPO}$) and their residence lifetime in the vesicles ($\tau^{INTRALIPO}$) [Eq. (3)]:

$$R_{1p}^{IN} = \left(\frac{\chi^{INTRALIPO}}{T_1^{INTRALIPO} + \tau^{INTRALIPO}}\right) \quad (3)$$

$T_1{}^{INTRALIPO}$ can be described in close analogy to what was reported for $R_{1p}{}^{OUT}$ [Eq. (2)], but considering that in the present case the amount of water in the compartment that contains the Gd complexes pointing inward of the vesicles ($\chi_{Gd}{}^{IN}$) corresponds to ($\chi^{INTRALIPO} \times 55.6$) [Eq. (4)]:

$$1/T_1^{INTRALIPO} = \left[\left(\frac{\chi_{Gd}^{IN} \times 10^{-3}}{\chi^{INTRALIPO} \times 55.6} \times \frac{1}{T_{1M} + \tau_M}\right) + R_{1OS}^{IN}\right] \quad (4)$$

If $\tau^{INTRALIPO}$ is negligible with respect to $T_1{}^{INTRALIPO}$, Equations (3) and (4) can be rearranged to give Equation (5), which assumes exactly the same form of Equation (2) and corresponds to the situation occurring when only a single water pool is present:

$$R_{1p}^{IN} = \left[\frac{\chi_{Gd}^{IN}}{55.6} \times \frac{1}{(T_{1M} + \tau_M)}\right] + R_{1OS}^{OUT} \quad (5)$$

Considering a homogeneous distribution of the amphiphilic complexes within the unilamellar bilayer, χ^{IN} and χ^{OUT} should correspond to the surface ratio between the inner and the outer leaflet.

For a sphere with an outer radius of 70 nm and a membrane thickness of 4 nm, such a ratio is equal to 1.16, thereby yielding values of 0.46 and 0.54 for χ^{IN} and χ^{OUT}, respectively. $\chi^{INTRALIPO}$ can be calculated by the product between the volume of water entrapped in a single vesicle ($V_{single}{}^{INTRALIPO}$) and the number of vesicles (N_{LIPO}) contained in a unitary volume of the suspension [Eq. (6)]:

$$V_{total}^{INTRALIPO} = V_{single}^{INTRALIPO} \times N_{LIPO} \quad (6)$$

$V_{single}{}^{INTRALIPO}$ is calculated from the external diameter of the vesicles as determined by dynamic light scattering (140 nm for both the samples investigated in this work) subtracted from the value of the bilayer thickness (4 nm).

N_{LIPO} is estimated on the basis of the surface area occupied by the components of the membrane [Eq. (7)]:

$$N_{LIPO} = \frac{S_{total}}{S_{single}} \quad (7)$$

The surface occupied by the membrane components of a single unilamellar liposome (S_{single}) can be assumed as the sum of the inner and outer leaflets of the bilayer.

The total surface occupied by the membrane components (S_{total}) can be estimated using the molecular surface area of the individual components and considering their concentration in the suspension. Under the assumption that the effective composition of the liposomes reflects the formulation (i.e., molar ratio 1,2-dipalmitoyl-*sn*-glycero-3-phosphocholine (DPPC)/cholesterol (Chol)/Gd complex (GdL)/1,2-distearoyl-*sn*-glycero-3-phosphoethanolamine-*N*-[methoxy (polyethylene glycol)-2000 (DSPE-PEG2000) (L = generic ligand) corresponding to 55:30:10:5), and considering a 1 mM total concentration of the incorporated Gd complexes, the millimolar concentration for the membrane components (the phospholipids DPPC and DSPE-PEG2000 were considered to contribute equally) in the suspension are [Eq. (8)]:

$$\begin{aligned}[GdL] &= 1\,mM;\ [DPPC + DSPE\text{-}PEG2000] = 1 \times \frac{60}{10} \\ &= 6\,mM;\ [Chol] = 1 \times \frac{30}{10} = 6\,mM\end{aligned} \quad (8)$$

Using a millimolar surface area of 3.5×10^{20}, 2.3×10^{20} and 4.8×10^{20} nm^2 for phospholipids, cholesterol, and Gd complexes, respectively,[20] the total membrane surface can be obtained from [Eq. (9)]:

$$S_{total} = \sum S_i[i] \quad (9)$$

Here, S_i refers to the millimolar surface area of the *i*-th component, and [*i*] is its millimolar concentration.

Finally, the residence lifetime of the water protons in the inner core of the vesicles ($\tau^{INTRALIPO}$) is dependent on the water

permeability of the liposome bilayer (P_W) and the vesicle size [Eq. (10)]:

$$\tau^{INTRALIPO} = \frac{r_{inner}}{3 \times P_W} \quad (10)$$

During the analysis of the NMRD profiles, the values of size, membrane thickness and the molar fraction of the membrane components were kept fixed. NMRD profiles were fitted only in the high-field region (>2 MHz) because of the known limitations of SBM theory to properly account for the behaviour of slowly tumbling systems at low magnetic field strengths.[21] The least-squares fitting of the data was performed by treating as variable parameters Δ^2, τ_V, τ_{RG}, τ_{RL}, τ_{RM}, S^2 and P_W. In addition, each parameter was allowed to vary only within a reasonable range of values typical of Gd^{III} complexes.

The results of the best-fit analyses are shown in Figure 2 for the two liposomal preparations investigated in this work and the values of the best-fit parameters are reported in Table 1.

Confirming the qualitative analysis made earlier, the results of the fitting prove that the residence lifetime τ_M is the parameter most affected by the nature of the Gd^{III} complex incorporated in the liposomes. The correlation between the structure of the chelate and the exchange rate of the coordinated water molecule has been thoroughly investigated in the recent past, so we can attribute the large difference observed to the different chemical nature of the donor atoms in the two chelates. In fact, the substitution of a carboxylic group with an amide moiety invariantly leads to a lengthening of τ_M as a result of the variation of the residual electrostatic charge from −1 ($GdDOTA(GAC_{12})_2$) to 0 ($GdDOTAMA(C_{18})_2$). However, it cannot be excluded that other additional factors (e.g., steric hindrance at the water binding site, structural effects caused by the incorporation in the liposome bilayer and so forth) may also contribute to the observed τ_M values, even though the value obtained for LIPO-$GdDOTA(GAC_{12})_2$ is quite similar to that reported for the water-soluble analogue (100 ns).[14] For these Gd-based macromolecular systems the parameters for electronic relaxation (Δ^2, τ_V) are simply empirical fitting parameters and do not assume a well-defined physical meaning. However, it can be noted that both parameters have a smaller value in the case of $GdDOTA(GAC_{12})_2$, in line with many empirical observations made on DOTA-like complexes and DOTA monoamide derivatives.[3c,22] As discussed earlier, the poor motional coupling between the paramagnetic unit and the nanoparticle is very relevant and markedly affects the relaxivity enhancement attainable. In fact, although the global rotation is quite similar for the two paramagnetic liposomes, the degree of local rotational motion is significantly higher in the case of LIPO-$GdDOTAMA(C_{18})_2$ (τ_{RL} = 0.44 vs. 1.70 ns) as also clearly indicated by the difference in the order parameter S^2.

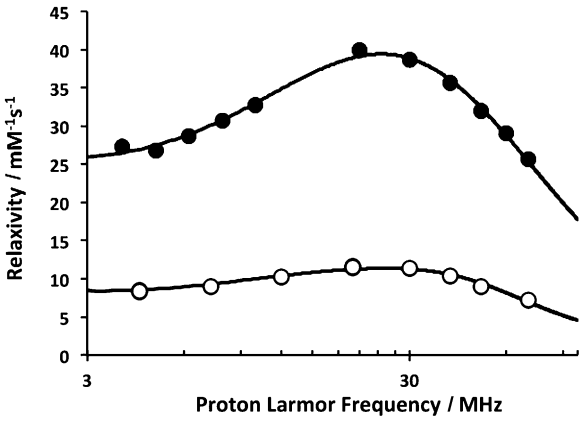

Figure 2. ^1H NMRD profiles at 25 °C of paramagnetic liposomes incorporating $GdDOTAMA(C_{18})_2$ (○) and $GdDOTA(GAC_{12})_2$ (●).

Table 1. Relaxation parameters (at 25 °C) obtained from the analysis of the NMRD profiles reported in Figure 2.[a]

Parameter	$GdDOTAMA(C_{18})_2$	$GdDOTA(GAC_{12})_2$
Δ^2 [10^{19} s^{-2}]	0.81 ± 0.1	0.65 ± 0.1
τ_V [ps]	29 ± 5	11 ± 4
τ_{RG} [ns]	82 ± 8	78 ± 10
τ_{RL} [ns]	0.44 ± 0.2	1.70 ± 0.3
τ_M [ns]	769 ± 45	120 ± 15
S^2	0.39 ± 0.09	0.64 ± 0.12
P_w [$\times 10^{-5}$ cm s^{-1}]	1.2 ± 0.5	15 ± 1.5

[a] The parameters for electronic relaxation (Δ^2, τ_V) were used as empirical fitting parameters and do not have a precise physical meaning for these macromolecular systems. The distance of the coordinated water molecule from the metal ion (r_{Gd-H}) was fixed to 3.0 Å. The outer-sphere component of the relaxivity was estimated by using standard values for the distance of closest approach a (4 Å) and the relative diffusion coefficient D of solute and solvent (2.24×10^{-5} $cm^2 s^{-1}$).

As far as the water permeability of the liposome bilayer is concerned, the much higher (almost one order of magnitude) value obtained for the bilayer embedded with $GdDOTA(GAC_{12})_2$ is noteworthy. This finding confirms previous observations indicating that the incorporation of amphiphilic chelates with lipophilic tails in different positions of the ligand favours an increase of the water diffusivity across the bilayer.[23]

In vivo MRI comparison between the liposomal agents on an experimental tumour model

On the basis of the promising in vitro results, we deemed it of interest to compare the in vivo performance of the two liposomal agents on an MRI scanner operating at 1 T (40 MHz). The experimental protocol consisted of injecting 200 μL of the liposomal suspension containing 0.05 mmol Gd kg^{-1} body weight in the tail vein of mice bearing a subcutaneous syngeneic B16 melanoma. The T_1 contrast was then monitored over time in selected organs (liver, spleen, kidneys and tumour).

Figure 3 shows three morphological T_{2w} MRI images of a representative mouse acquired before injecting the liposomal agents, to display the attainable anatomical resolution in monitoring the contrast in the organs of interest (tumour, liver, spleen and kidneys).

Figure 4 illustrates some representative T_{1w} images acquired 10 min after the administration of the paramagnetic liposomes. A general brightening owing to the presence of the paramag-

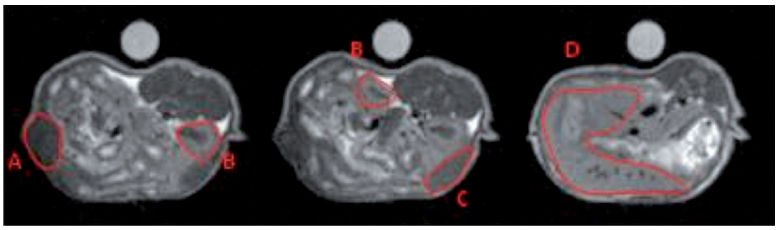

Figure 3. 1 T MRI T_{2w} images of three axial slices of a mouse prior to the injection of the paramagnetic liposomes. The organs circled in red are: tumour (A), kidney (B), spleen (C) and liver (D).

netic species is detectable in liver, spleen and kidneys. An accurate comparison between the imaging performances of the two agents is possible by means of a careful assessment of the T_1 contrast enhancement in the various organs. Figure 5 summarises the obtained results. A first clear piece of evidence is that the contrast detected up to 4–5 h after the injection of the liposomes loaded with GdDOTA(GAC_{12})$_2$ was much higher than the corresponding values measured in all the considered organs for the nanovesicles loaded with GdDOTAMA(C_{18})$_2$. Under the reasonable assumption that the biodistribution of the two types of liposomes in the organ is almost identical (justified by the same size of the two vesicles), the superior MRI detectability of LIPO-GdDOTA-(GAC_{12})$_2$ was about two-fold, consistent with the four-fold higher relaxivity observed in vitro. It is likely that such a difference may be explained in terms of: 1) the different temperatures between in vitro (25 °C) and in vivo (32–33° for an anesthetised mouse)[24] conditions; 2) the in vivo compartmentalisation effects (the agent is not homogeneously distributed among the biological compartments of the tissue); and 3) the fact that the signal is weighted on T_1 and thus not uniquely dependent on the effective T_1. All these factors can contribute to reduce the in vivo performance of the MRI probe.

Figure 5 shows the changes of T_1 contrast over time. The enhancement observed for LIPO-GdDOTA(GAC_{12})$_2$ decreased markedly after about 7 h, significantly more rapidly than for LIPO-GdDOTAMA(C_{18})$_2$. Remarkably, at about 10 h post-injection the LIPO-GdDOTA(GAC_{12})$_2$ contrast enhancement is lower than that of the less efficient agent.

The rapid T_1 contrast decrease showed by LIPO-GdDOTA-(GAC_{12})$_2$ suggests a faster clearance rate of the incorporated agent, or it could be caused by an intra-organ liposome degradation with formation of paramagnetic species of lower relaxivity.

To gain more insight into these hypotheses, the amount of the paramagnetic ion was measured by inductively coupled plasma mass spectrometry (ICP-MS) on organs explanted 1.5, 5 and 24 h post-injection of the liposomes. The data are reported in Figure 6. The amount of Gd found in the organs (normalised to the organ weight) for the two agents at 1.5 h post-injection was similar in liver and kidneys, whereas some small differences were detected in spleen and tumour. Figure 7 reports the comparison between the percentage variation of MRI contrast and ICP-MS data, both taken at 1.5 h post-injection, of LIPO-GdDOTA(GAC_{12})$_2$ over LIPO-GdDOTAMA(C_{18})$_2$ agents (i.e.,

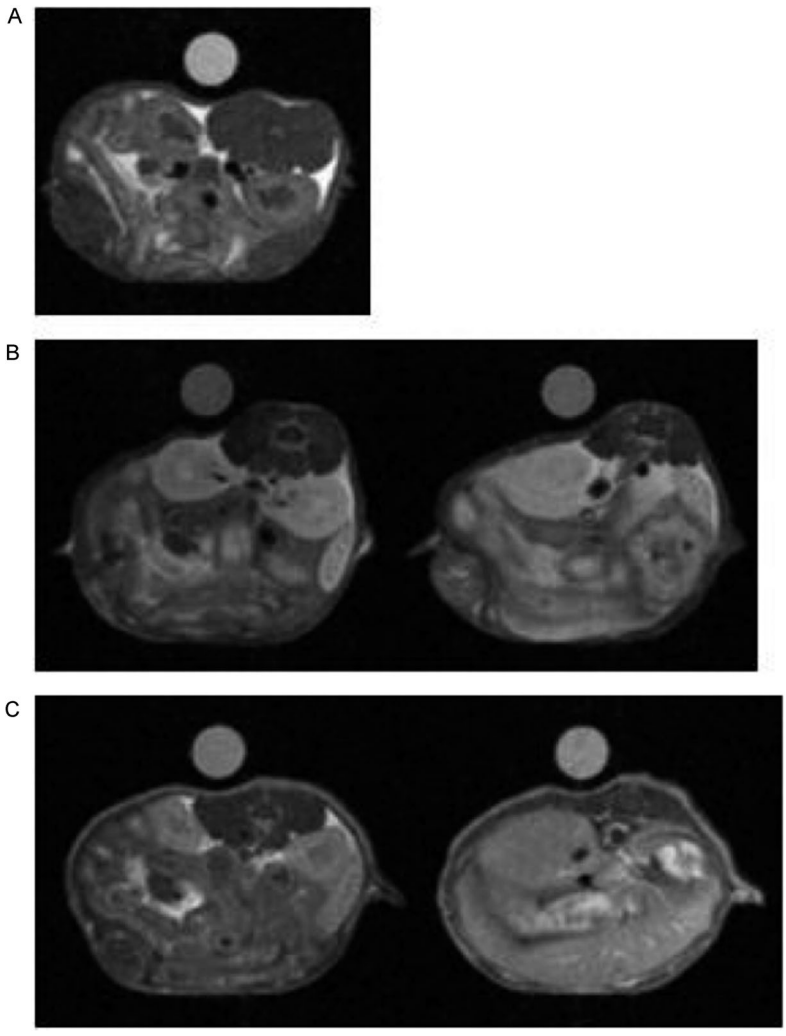

Figure 4. MRI T_{1w} images. A) Pre-injection, (B) 10 min after injection of GdDOTA(GAC_{12})$_2$-loaded liposomes, (C) 10 min after injection of the GdDOTAMA(C_{18})$_2$-loaded liposomes.

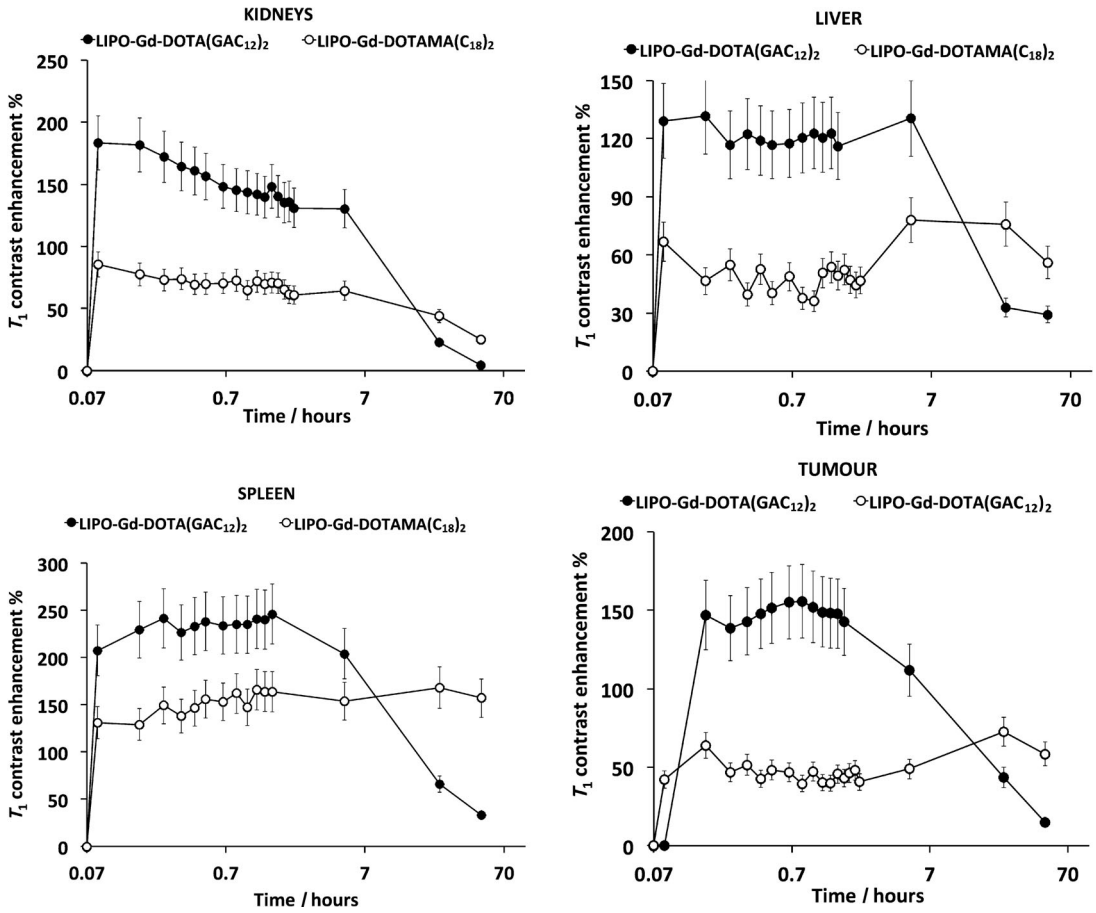

Figure 5. Time evolution of the T_1 contrast enhancement in the indicated organs after injection of paramagnetic liposomes incorporating GdDOTAMA(C_{18})$_2$ (○) and GdDOTA(GAC_{12})$_2$ (●).

[(MRI_{C12}−MRI_{C18})/MRI_{C18}]×100). The bar plot highlights the correlation between the relative quantification (ICP-MS) and contrast efficiency (MRI) of the two agents. For instance, in kidneys, the two liposomes displayed a quite similar Gd concentration, with a little preference for LIPO-GdDOTAMA(C_{18})$_2$. However, the use of nanovesicles loaded with GdDOTA(GAC_{12})$_2$ led to a much higher contrast. This finding is a clear indication of the intrinsic higher relaxometric efficacy of this amphiphilic probe. Surprisingly, the organs of the mononuclear phagocyte system, that is, spleen and liver, showed a preferential avidity for LIPO-GdDOTAMA(C_{18})$_2$, but the MRI contrast observed for LIPO-GdDOTA(GAC_{12})$_2$ was still higher and, moreover, it was well correlated with the decrease of the differential uptake between LIPO-GdDOTA(GAC_{12})$_2$ and LIPO-GdDOTAMA(C_{18})$_2$ observed on passing from liver to spleen. Most likely the reduced localisation in liver and spleen allowed a preferential accumulation of LIPO-GdDOTA(GAC_{12})$_2$ agent in the tumour, for which the agent showed the highest contrast enhancement (ca. 250%) relative to LIPO-GdDOTAMA(C_{18})$_2$.

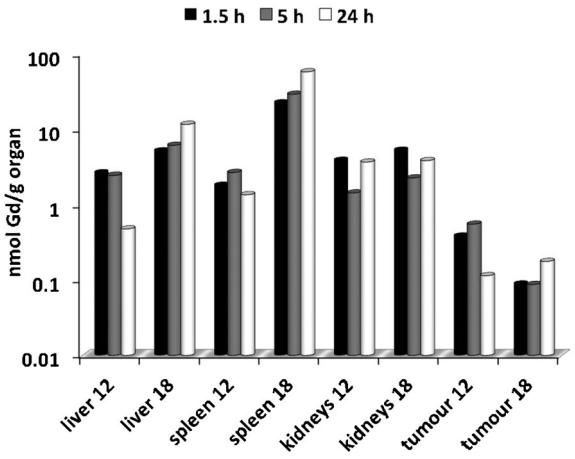

Figure 6. Amount of gadolinium measured by ICP-MS, normalised to the organ weight, found for the different organs excised from mice injected with LIPO-GdDOTAMA(C_{18})$_2$ or LIPO-GdDOTA(GAC_{12})$_2$ as a function of the time post-injection.

As far as the clearance rate is concerned, the data reported in Figure 6 indicate that GdDOTA(GAC_{12})$_2$ is eliminated much faster than the agent with the longer aliphatic chains, with the exception of kidneys, for which the two systems showed similar kinetic profiles. Graphically, this result can be better represented as the ratio between the amount of Gd determined by ICP-MS at 5 and 24 h normalised to the value obtained at 1.5 h post-injection (Figure 8). The data reported in the plot highlight the difference in the kinetic behaviour for the two liposo-

mal samples in the investigated organs. This finding is a strong indication of the more rapid clearance of the imaging agent conjugated with the shorter aliphatic chains and with a residual negative charge. On the other hand, the close similarity between the kinetic profiles of the agents in the kidneys could be justified by a predominant intravascular distribution in this organ with no, or negligible, renal accumulation. In fact, in this case, it is reasonable to assume that the blood circulation lifetime of the two liposomal agents is similar. Thus, the different kinetic profiles obtained for the two complexes can allow the identification of the tissues at which the liposomes extravasate and accumulate.

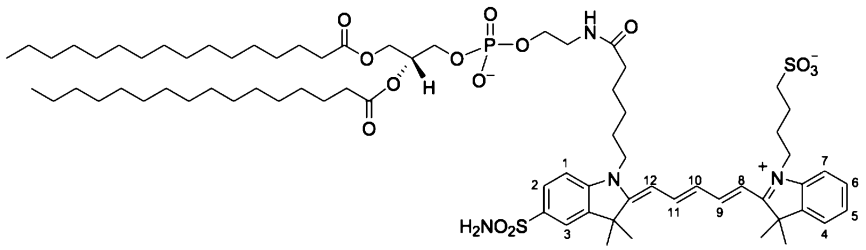

Scheme 2. Chemical structure of Cy5-$(C_{16})_2$ with numbering scheme adopted for ^{1}H NMR assignment (see Experimental Section).

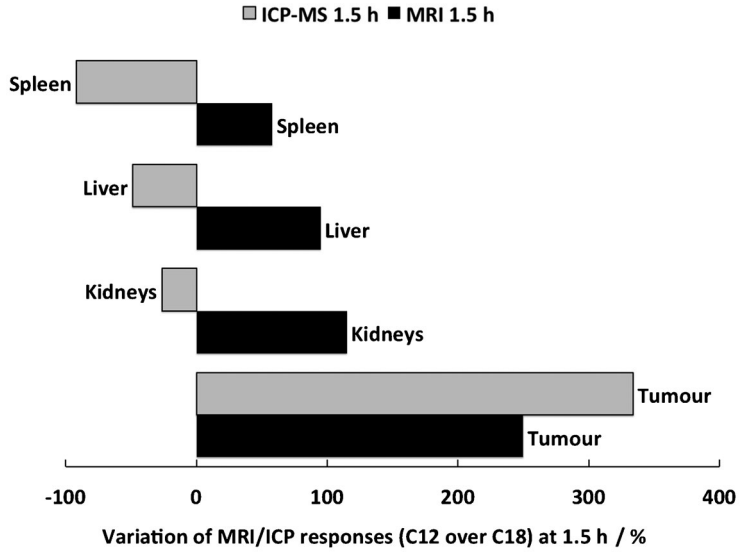

Figure 7. Variation of MRI T_1 contrast and ICP-MS data calculated, at 1.5 h post-injection, from the values reported in Figures 4 and 5 by using the following formula (in the case of MRI): $[(MRI_{C12}-MRI_{C18})/MRI_{C18}]\times 100$.

To gain further information on the biodistribution of the two liposomal agents, the nanovesicles were additionally loaded with a newly synthesised amphiphilic phospholipid-like fluorescent dye, Cy5-$(C_{16})_2$, based on cyanine fluorophore and conjugated with two palmitic aliphatic chains (Scheme 2). The results, expressed as nanomoles of dye per gram of organ, are shown in Figure 9, which reports the temporal variation of the uptake normalised to the uptake at 1.5 h (as done in Figure 8). The two preparations were injected into tumour-bearing mice and the organs were excised after 1.5, 5 and 24 h to be analysed by spectrofluorimetry.

The data reported in Figure 9 confirmed that liver and spleen were the organs with the highest liposome uptake. However, the excretion kinetics of the liposome loaded with the fluorescent dye was quite

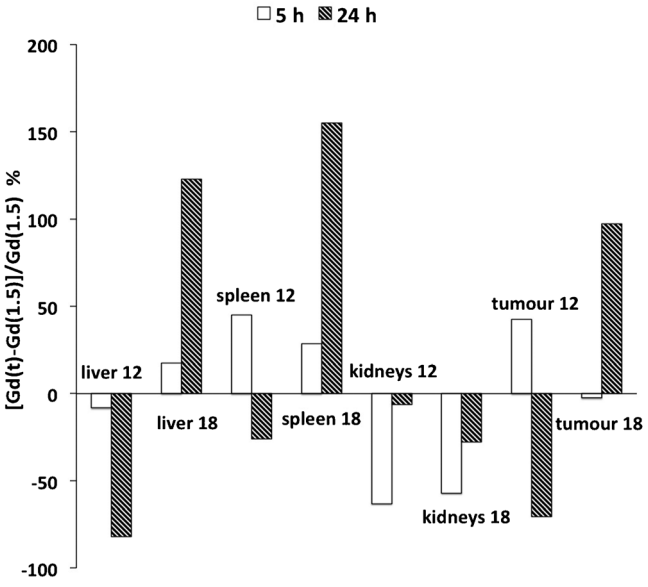

Figure 8. Percentage variation of the amount of Gd determined at 5 and 24 h post-injection normalised to the value determined after 1.5 h.

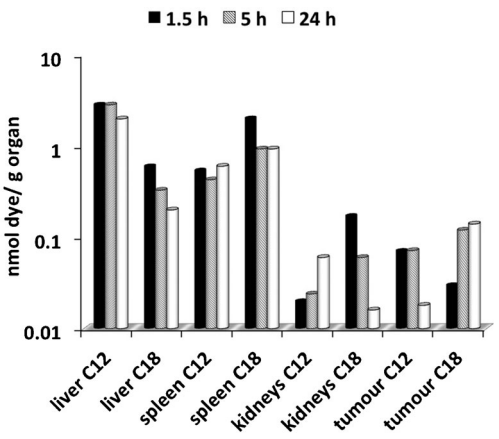

Figure 9. Spectrophotometric quantification of GdDOTAMA$(C_{18})_2$ and GdDOTA(GAC_{12}) liposomes loaded with Cy5-$(C_{16})_2$ dye in mice organs. Organs of treated mice were excised at different times after administration and the fluorescence was quantified with a standard curve and normalised to organ weight.

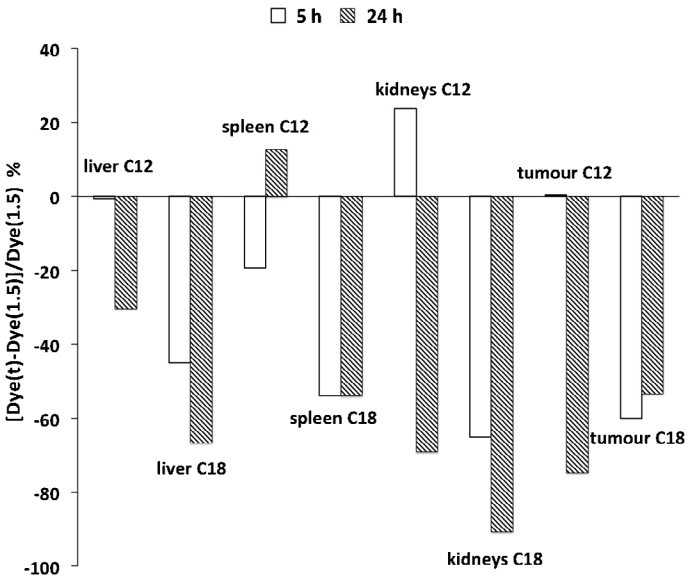

Figure 10. Percentage variation of the amount of Cy5-$(C_{16})_2$ determined at 5 and 24 h post-injection with respect to the uptake determined after 1.5 h.

similar to that determined for the dye-free liposomes loaded with GdDOTA$(GAC_{12})_2$, and different from that of GdDOTAMA-$(C_{18})_2$-loaded vesicles, especially in liver and spleen (Figures 7 and 8 versus Figures 9 and 10). This observation may indicate that, in addition to vesicle degradation, the removal of the amphiphilic compounds from the organs could occur through the separation of the hydrophilic moiety (Gd complexes or Cy5-based dye).

According to this hypothesis, the data indicate that the stability of the linkage between lipophilic and hydrophilic portions of the amphiphiles decreases in the order GdDOTAMA-$(C_{18})_2$ > GdDOTA$(GAC_{12})_2 \approx$ Cy5-$(C_{16})_2$.

Conclusion

Relatively minor differences in the molecular structure of two amphiphilic Gd-containing agents determine marked differences in either the induced T_1 contrast or the excretion pathway on incorporating these species into liposomes.

The two considered systems contain GdDOTA-like agent bearing short hydrophobic chains (C_{12}), suitably designed to display an optimal rate of water exchange and restricted local rotational dynamics (LIPO-GdDOTA$(GAC_{12})_2$), and an amphiphilic Gd^{III} agent conjugated with C_{18} chains (LIPO-GdDOTAMA-$(C_{18})_2$) as a reference. On embedding these complexes into the liposome membrane, the determinants of the observed relaxivity are the occurrence of a slow tumbling motion (long τ_{RG}), the effect of which may be eventually "quenched" by the occurrence of a long water residence lifetime. The T_1 contrast is markedly higher for the complex endowed with a residual negative charge, which determines a faster exchange rate for the coordinated water molecule. In addition, a pronounced advantage in terms of restricted local mobility is observed for GdDOTA$(GAC_{12})_2$, which also plays an important role in determining the higher relaxivity.

The two Gd-loaded liposomes were then labelled with a Cy5-based fluorescent dye (bound to a C_{16} phospholipid) and the excretion kinetics were similar to those of LIPO-GdDOTA$(GAC_{12})_2$ and faster than for LIPO-GdDOTAMA$(C_{18})_2$. This finding suggests that, in addition to the stability of the incorporation in the vesicles, the removal of the imaging probes from the organs might occur through the detachment of the polar portion of the amphiphiles.

Taken together, the results presented herein indicate that liposomes loaded with GdDOTA$(GAC_{12})_2$ may have great potential for molecular MRI by virtue of their favourable relaxometric and pharmacokinetic properties.

Experimental Section

Chemicals

1,2-Dipalmitoyl-sn-glycero-3-phosphoethanolamine (DPPE), 1,2-Dipalmitoyl-*sn*-glycero-3-phosphocholine (DPPC), 1,2-distearoyl-*sn*-glycero-3-phosphoethanolamine-*N*-[methoxy (polyethylene glycol)-2000] ammonium salt (DSPE-PEG2000) and cholesterol (Chol) were purchased from Avanti Polar Lipids Inc. (Alabaster, AL, USA). GdDOTAMA$(C_{18})_2$ and GdDOTA$(GAC_{12})_2$ complexes were synthesised according to the procedures reported in references [13] and [14], respectively. Cy5 dye was kindly supplied by Ferrania Technologies S.p.A. (Cairo Montenotte, SV, Italy). All other chemicals were purchased from Sigma–Aldrich. Culture medium RPMI 1640, biological buffers, and foetal bovine serum were purchased from Cambrex, East Rutherford, NJ.

Synthesis of Cy5-*N*-hydroxysuccinimide

A solution of dye Cy5 (0.200 g, 0.29 mmol) and *N*-hydroxysuccinimide (0.050 g, 0.43 mmol) in dry DMF (3 mL) was cooled to 0 °C and a solution of *N*-ethyl-*N*′-[3-(dimethylamino)propyl]carbodiimide hydrochloride (0.082 g, 0.43 mmol) in dry DMF (0.5 mL) was added in 5 min. The mixture was stirred for 20 h at room temperature, washed with water (3×15 mL), dried and used without further purification.

Synthesis of Cy5-$(C_{16})_2$

A solution of Cy5-*N*-hydroxysuccinimide in dry CH_2Cl_2 (1 mL) was added slowly, at room temperature, to a solution of DPPE (0.020 g, 0.029 mmol) in dry CH_2Cl_2 (5 mL) and triethylamine (0.029 mmol, 4 mL). The product was recovered after purification by column chromatography (silica gel, elution gradient: CH_2Cl_2/MeOH 95:5→9:1→8:2; TLC: CH_2Cl_2/MeOH, 9:1 (v/v), R_f = 0.22) to yield a dark blue solid. A 56% pure product was obtained (22 mg). ^{1}H NMR (CD_3OD, 600 MHz): δ = 8.36 (t, ^3J(H,H) = 12.90 Hz, 1H; *H9*), 8.24 (t, ^3J(H,H) = 13.24 Hz, 1H; *H11*), 7.95 (d, ^3J(H,H) = 8.45 Hz, 1H; *H2*), 7.93 (s, 1H; *H3*), 7.58 (d, ^3J(H,H) = 7.99 Hz, 1H; *H4*), 7.51 (m, 2H; *H6*, *H7*), 7.35 (m, 2H; *H1*,*H5*), 6.75 (t, ^3J(H,H) = 12.23 Hz, 1H; *H10*), 6.60 (d, ^3J(H,H) = 13.87 Hz, 1H; *H8*), 6.26 (d, ^3J(H,H) = 13.48 Hz, 1H; *H12*), 5.25 (s, 1H; *glycerol*), 4.46 (d, ^3J(H,H) = 13.19 Hz, 2H), 4.30 (m, 2H), 4.21 (m, 2H), 4.10 (m, 2H), 4.01 (m, 2H), 3.92 (m, 2H), 3.41 (m, 2H), 2.92 (m, 2H), 2.34 (m, 4H), 2.26 (m, 2H), 2.06 (m, 2H), 1.98 (m, 2H), 1.84 (m, 2H), 1.78 (s, 12H; CH_3 indole), 1.73 (m, 2H), 1.61 (m, 4H),

1.50 (m, 2H), 1.30 (m, 48H), 0.93 ppm (m, 6H; CH_3, C_{16} chain); ESI-MS: *m/z* calcd ($M+H^+$) 1356.78; found: 1356.77.

Liposome preparation

Long-circulating liposomes were prepared as described previously.[14] The total amount of phospholipids and amphiphilic complex was 60 mg mL^{-1}. Briefly, appropriate amounts of DPPC, cholesterol, DSPE-PEG2000, and GdDOTAMA(C_{18})$_2$ or GdDOTA(GAC_{12})$_2$ in a molar ratio of 55:30:5:10, respectively, were dissolved in chloroform/methanol (95:5 by volume) in a round-bottomed flask. A lipid film was prepared after slow solvent removal under reduced pressure on a rotary evaporator. The film was then dried under a stream of nitrogen for 2 h. Liposomes were formed by adding an isotonic buffer at pH 7.4, composed of 10 mM 4-(2-hydroxyethyl)-1-piperazineethanesulfonic acid (HEPES) and 135 mM NaCl, to the lipidic thin film. The hydration was performed at 55 °C and was accompanied by vigorous shaking. The obtained suspension was extruded several times (Lipex extruder, Northern Lipids Inc.) through polycarbonate filters with progressively reduced pore diameters from 400 to 100 nm. Liposomes were dialysed briefly (4 h) to remove any non-incorporated material. The mean hydrodynamic size of the liposomes was determined by dynamic light scattering (Zetasizer Nano 90 ZS, Malvern, UK) and was found to be around 140 nm with a polydispersity index value lower than 0.2. The total concentration of the paramagnetic complexes in the liposome suspension was determined by magnetic susceptibility measurements.[14]

^{1}H NMR relaxation measurements

The magnetic field dependence of the water proton longitudinal relaxation rates for the buffered (see above) suspensions of the paramagnetic complexes incorporated in the liposomes were measured on a fast field-cycling Stelar SmarTracer relaxometer (Stelar s.r.l., Mede, Pv, Italy) over a continuum of magnetic field strengths from 0.00024 to 0.25 T (corresponding to 0.01–10 MHz proton Larmor frequencies). The relaxometer was operated under computer control with an absolute uncertainty in $1/T_1$ of ±1%. Additional data points in the range 15–70 MHz were obtained on a Bruker WP80 NMR electromagnet adapted to variable-field measurements (15–80 MHz proton Larmor frequency) with a Stelar relaxometer. The exact concentration of Gd^{III} was determined by measurement of bulk magnetic susceptibility shifts of a *t*BuOH signal. The ^{1}H T_1 relaxation times were acquired by the standard inversion recovery method with a typical 90° pulse width of 3.5 μs and 16 experiments of four scans. The reproducibility of the T_1 data was ±5%. The temperature was controlled with a Stelar VTC-91 airflow heater equipped with a calibrated copper–constantan thermocouple (uncertainty of ±0.1 °C).

Cells

B16.F10 murine melanoma cells were cultured as monolayers at 37 °C in a 5% CO_2-containing humidified atmosphere in RPMI 1640 medium supplemented with 10% (vol/vol) heat-inactivated foetal calf serum, 100 IU mL^{-1} penicillin and 100 mg mL^{-1} streptomycin.

Mouse model

Male C57Bl/6 mice (6–8 weeks of age) were obtained from Charles River Laboratories (Calco, Italy) and kept in housing with standard rodent chow and water available ad libitum, and a 12 h light/dark cycle. Experiments were performed according to the national regulations and were approved by the local animal experiments ethical committee. For tumour induction, 1 million B16.F10 melanoma cells dispersed in phosphate-buffered saline (0.2 mL) were inoculated subcutaneously in the right flank of the mouse. Around 1 week after cell inoculation, the mice developed solid tumours of size around 20 mm^3 and they were subjected to imaging experiments. For MRI acquisition, the mice were anaesthetised by injecting tiletamine/zolazepam (20 mg kg^{-1}; Zoletil 100; Virbac, Milan, Italy) and xylazine (5 mg kg^{-1}; Rompun; Bayer, Milan, Italy). Mice received a single intravenous injection (caudal vein) of liposomes corresponding to 0.05 mmol Gd kg^{-1} body weight.

MRI measurements

The animals (four for each liposomal preparation) were subjected to MRI investigation before injection of Gd–liposomes, within 2 h post-injection, and then after 6, 24 and 48 h. MR images were acquired at 1 T on an Aspect M2 High-Performance MRI System (Aspect Magnet Technologies Ltd., Netanya, Israel), mounted with a NdFeB permanent magnet with a field homogeneity of 0.2–0.5 G. This system was equipped with a 35 mm solenoid Tx/Tr coil (inner diameter 35 mm) and fast gradient coils (gradient strength: 450 mT m^{-1} at 60 A; ramp time: 250 μs at 160 V). MR images were acquired using a standard T_1-weighted multislice spin-echo sequence, with a flip angle of 90°, repetition time (TR)/time to echo (TE)/number of acquisitions (NEX) = 200:6:10, field of view (FOV) = 4.0×4.0 cm, data matrix 128×128, slice thickness 1.5 mm, interslice distance 0.1 mm, slice number 11. T_1 contrast was calculated as a percentage (T_1^{enh}%, enh = enhanced) by using Equation (11):

$$T_1^{enh}\% = \frac{I_{POST} - I_{PRE}}{I_{PRE}} \times 100 \qquad (11)$$

in which I_{PRE} and I_{POST} are the MR signal intensity of a manually drawn region of interest, normalised with respect to an external reference, before and after the intravenous injection of the liposomes, respectively. Contrast was measured in liver, spleen, tumour and kidneys.

Ex vivo determination of liposome biodistribution

To evaluate the biodistribution of the injected liposomes and the MRI data obtained in parallel, the amount of material delivered by the nanovesicles to the given organs was determined ex vivo after excising liver, spleen, kidneys and tumour. Two analytical methods were used: spectrofluorimetry and ICP-MS. The former approach required the incorporation of Cy5-(C_{16})$_2$ fluorescent dye in the liposome bilayer (5% in moles of the lipid components). The amount of Gd^{III} distributed in the organs over time was determined by ICP-MS. Each excised organ was weighed, chopped with a scalpel, placed in a vial with a solution of methanol and chloroform (50:50), and finally homogenised with Ultra-Turrax. A series of centrifugations were performed to give a clear solution. Then, each solution was subjected to spectrofluorimetric analysis (FluoroMax-4, Horiba Jobin Yvon) and the concentration was read from a calibration curve of the dye dissolved in chloroform/methanol. The dye was excited at 650 nm and fluorescence was detected at 671 nm. As the fluorescent dye can primarily act as reporter of the liposome distribution, it is important to evaluate directly the amount of gadolinium distributed in the organs over time. ICP-MS (ELAN

6100, PerkinElmer) was selected as a highly sensitive analytical technique to achieve this objective. The samples were mineralised in a microwave vessel (Mars-5 Xpress, C.E.M.) by using nitric acid 60%.

Acknowledgements

Financial support from Regione Piemonte (Nano-IGT and PIIMDMT Projects) and MIUR (PRIN 2009) is gratefully acknowledged. This study was performed under the auspices of the Consorzio Interuniversitario di Ricerca in Chimica dei Metalli nei Sistemi Biologici (CIRCMSB) and EU-COST Action TD1004.

Keywords: gadolinium · imaging agents · liposomes · relaxometry · tumour uptake

[1] a) I. R. Young, *Methods in Biomedical Magnetic Resonance Imaging and Spectroscopy*, Wiley, Chichester, **2000**; b) P. A. Rinck, *Magnetic Resonance in Medicine*, Wiley, Chichester, **2001**.
[2] a) D. Sosnovik, R. Weissleder, *Prog. Drug Res.* **2005**, *62*, 83; b) E. Terreno, D. Delli Castelli, A. Viale, S. Aime, *Chem. Rev.* **2010**, *110*, 3019–3042.
[3] a) A. E. Merbach, È. Tóth, *The Chemistry of Contrast Agents in Medical Magnetic Resonance Imaging*, Wiley, Chichester, **2001**; b) S. Aime, M. Botta, E. Terreno, *Adv. Inorg. Chem.* **2005**, *57*, 173–237; c) P. Caravan, J. J. Ellison, T. J. McMurry, R. B. Lauffer, *Chem. Rev.* **1999**, *99*, 2293–2352.
[4] a) D. L. J. Thorek, A. K. Chen, J. Czupryna, A. Tsourkas, *Ann. Biomed. Eng.* **2006**, *34*, 23–38; b) Y. X. Wang, *Quant. Imaging Med. Surg.* **2011**, *1*, 35–40; c) S. Laurent, D. Forge, M. Port, A. Roch, C. Robic, L. Vander Elst, R. N. Müller, *Chem. Rev.* **2008**, *108*, 2064–2110.
[5] M. Botta, L. Tei, *Eur. J. Inorg. Chem.* **2012**, 1945–1960.
[6] a) D. Delli Castelli, E. Gianolio, S. Geninatti Crich, E. Terreno, S. Aime, *Coord. Chem. Rev.* **2008**, *252*, 2424–2443; b) A. J. L. Villaraza, A. Bumb, M. W. Brechbiel, *Chem. Rev.* **2010**, *110*, 2921–2959.
[7] a) A. Albanese, P. S. Tang, W. C. Chan, *Annu. Rev. Biomed. Eng.* **2012**, *14*, 1–16; b) A. E. Nel, L. Mädler, D. Velegol, T. Xia, E. M. Hoek, P. Somasundaran, F. Klaessig, V. Castranova, M. Thompson, *Nat. Mater.* **2009**, *8*, 543–557.
[8] a) A. Accardo, D. Tesauro, A. Luigi, C. Pedone, G. Morelli, *Coord. Chem. Rev.* **2009**, *253*, 2193–2213; b) W. J. M. Mulder, G. J. Strijkers, G. A. F. Van Tilborg, A. W. Griffioen, K. Nicolay, *NMR Biomed.* **2006**, *19*, 142–164; c) E. Terreno, D. Delli Castelli, C. Cabella, W. Dastrù, A. Sanino, J. Stancanello, L. Tei, S. Aime, *Chem. Biodiversity* **2008**, *5*, 1901–1912.
[9] H. Maeda, *Adv. Enzyme Regul.* **2001**, *41*, 189–207.
[10] E. Terreno, F. Uggeri, S. Aime, *J. Controlled Release* **2012**, *161*, 328.
[11] I. Bertini, F. Bianchini, L. Calorici, S. Colagrande, M. Fragai, A. Franchi, O. Gallo, C. Gavazzi, C. Luchinat, *Magn. Reson. Med.* **2004**, *52*, 669.
[12] L. Lattuada, A. Barge, G. Cravotto, G. B. Giovenzana, L. Tei, *Chem. Soc. Rev.* **2011**, *40*, 3019–3049.
[13] P. L. Anelli, L. Lattuada, V. Lorusso, M. Schneider, H. Tournier, F. Uggeri, *MAGMA* **2001**, *12*, 114.
[14] F. Kielar, L. Tei, E. Terreno, M. Botta, *J. Am. Chem. Soc.* **2010**, *132*, 7836–7837.
[15] a) S. Aime, M. Botta, M. Fasano, E. Terreno, *Acc. Chem. Res.* **1999**, *32*, 941–949; b) L. Helm, G. M. Nicolle, A. E. Merbach, *Adv. Inorg. Chem.* **2005**, *57*, 327–379.
[16] Z. Zhang, M. T. Greenfield, M. Spiller, T. J. McMurry, R. B. Lauffer, P. Caravan, *Angew. Chem.* **2005**, *117*, 6924–6927; *Angew. Chem. Int. Ed.* **2005**, *44*, 6766–6769.
[17] J. P. H. Freed, *J. Chem. Phys.* **1978**, *68*, 4034–4037.
[18] a) G. Lipari, S. Szabo, *J. Am. Chem. Soc.* **1982**, *104*, 4546–4559; b) G. Lipari, S. Szabo, *J. Am. Chem. Soc.* **1982**, *104*, 4559–4570.
[19] S. L. Fossheim, A. K. Fahlvik, J. Klaveness, R. N. Muller, *Mag. Res. Imaging* **1999**, *17*, 83–89.
[20] Cross section values were determined in silico using MOE software.
[21] a) J. S. Troughton, M. T. Greenfield, J. M. Greenwood, S. Dumas, A. J. Wiethoff, J. Wang, M. Spiller, T. J. McMurry, P. Caravan, *Inorg. Chem.* **2004**, *43*, 6313–6323; b) M. F. Ferreira, B. Mousavi, P. M. Ferreira, C. I. O. Martins, L. Helm, J. A. Martins, C. F. G. C. Geraldes, *Dalton Trans.* **2012**, *41*, 5472–5475.
[22] S. Aime, P. L. Anelli, M. Botta, F. Fedeli, M. Grandi, P. Paoli, F. Uggeri, *Inorg. Chem.* **1992**, *31*, 2422–2428.
[23] E. Terreno, A. Sanino, C. Carrera, D. Delli Castelli, G. B. Giovenzana, A. Lombardi, R. Mazzon, L. Milone, M. Visigalli, S. Aime, *J. Inorg. Biochem.* **2008**, *102*, 1112.
[24] D. K. Taylor, *J. Am. Assoc. Lab. Anim. Sci.* **2007**, *46*, 37–41.

Received: March 15, 2013
Published online on ■■ ▮▮, 0000